

QUIET HYDRAULIC ACTUATORS FOR LIGO

C Hardham, B Abbott, R Abbott, G Allen, R Bork, C Campbell, K Carter, D Coyne, D DeBra, T Evans, J Faludi, A Ganguli, J Giaime, M Hammond, W Hua, J Kern, J LaCour, B Lantz, M Macinnis, K Mailand, K Mason, R Mittleman, J Nichol, J Niekerk, B O'Reilly, D Ottaway, H Overmier, C Parameswariah, J Phinney, B Rankin, N A Robertson, D Sellers, P Sarin, D H Shoemaker, O Spjeld, G Traylor, S Wen, R Wooley, M Zucker

1 INTRODUCTION

The Laser Interferometer Gravitational-wave Observatory (LIGO) is a set of terrestrial based interferometers (Figure 1) constructed to detect gravitational waves. The LIGO Laboratory has built and operates two observatories in the United States, and several other countries have commissioned similar detectors around the world.

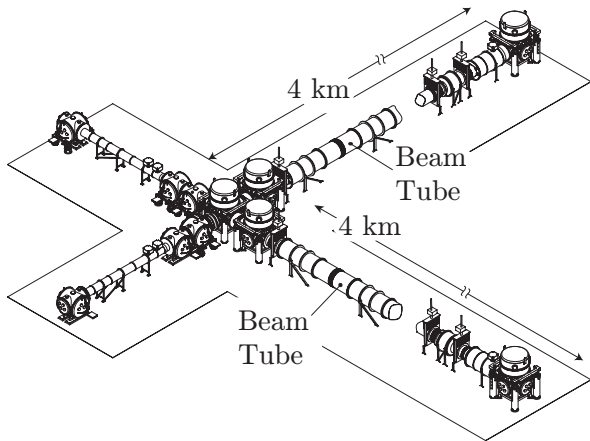


Figure 1: The LIGO detector; there are sites in Hanford, Washington and Livingston, Louisiana. The beam tubes contain one arm of the interferometer and the tanks at the end of the beam tubes contain the suspension systems and test masses.

Interferometric gravitational wave detection relies on precisely monitoring the distance between the *test masses* at the end of each arm which, conveniently, also serve as the end mirrors of the interferometer. For terrestrial detectors, this measurement is corrupted by seismic noise that is several orders of magnitude larger than the anticipated gravitational wave induced motion [1]. To reduce this disturbance and maintain the test mass at its operating point, the test mass is suspended from an alignment and isolation system. This system consists of several stages of isolation to effectively mitigate broadband seismic disturbances (Figure 2). The test mass hangs from a passive pendulum system which is supported by a multi-stage isolation and alignment system. At the Livingston site, external to the vacuum system, is the pre-isolator

system which is intended to suppress large amplitude, low-frequency disturbances and maintain the interferometer at its operating point. This paper focuses on the design of the pre-isolator actuator and the control of the pre-isolator system.

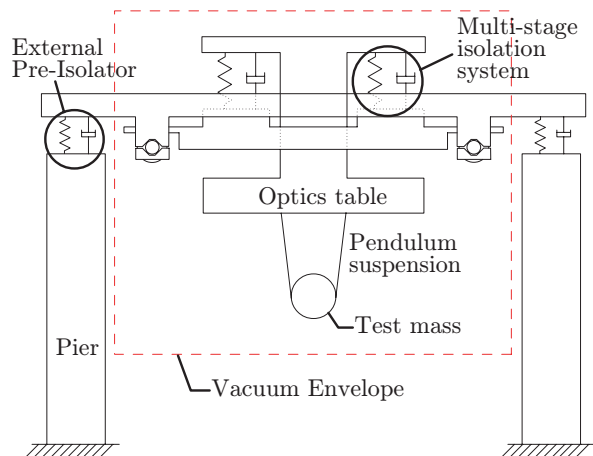


Figure 2: A schematic of a suspension system typical of the end chambers of the LIGO observatory.

Based on predictions for low-frequency disturbances and other specifications of the complete suspension and isolation system [2] [3], the requirements for the pre-isolator system actuator are challenging. Four specifications define this challenge:

- 1) maximum force of at least 2000 N,
- 2) throw of ± 1 mm,
- 3) bandwidth from zero frequency to at least 10 Hz,
- 4) noise not to exceed 10^{-9} m/ $\sqrt{\text{Hz}}$ at 1 Hz.

Several varieties of actuator were considered for this application. Mechanical actuators (screws/gears) were dismissed because of the non-linear, stick-slip behavior and noise inherent to mechanical connections. Piezoelectric actuators cannot provide enough throw. An electromagnetic actuator can meet many of the specifications, but poor impedance matching with the payload (Figure 3) combined with the power dissipated while holding DC offsets suggests that this would be a poor candidate.

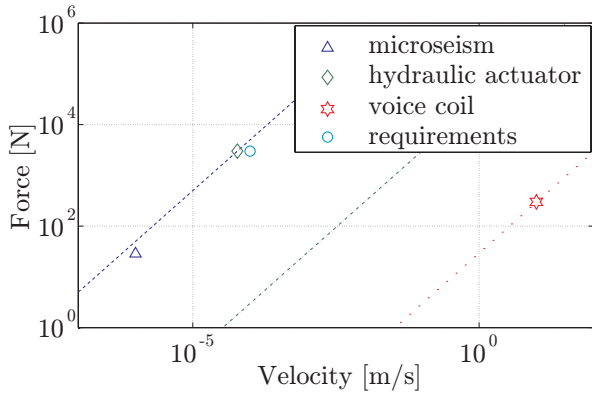


Figure 3: A plot of mechanical impedance for various actuators and the micro-seismic peak (the predominant low-frequency feature of the seismic spectrum). Also shown are lines of constant mechanical impedance. Note that the impedance of the hydraulic actuator nearly matches that of the micro-seismic peak and the requirements whereas the electromagnetic actuator is five orders of magnitude lower.

As an alternative, a quiet hydraulic actuator offers reasonable force and displacement with much lower noise than conventional hydraulics. Hence, the quiet hydraulic actuator is one known solution that is well matched with the requirements.

1.1 QUIET HYDRAULICS

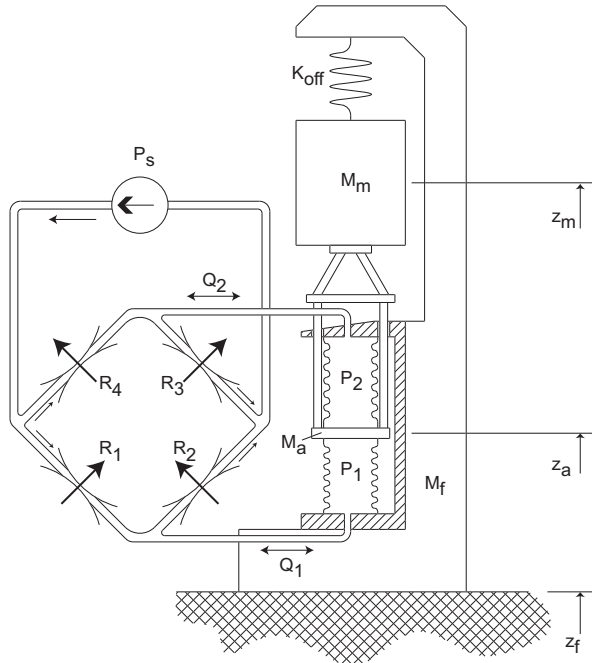


Figure 4: The actuator is composed of five principal parts. The pump, P_s , provides constant volumetric flow. The flow is sent through a servo valve that contains a Wheatstone bridge with variable resistances R_1 , R_2 , R_3 and R_4 , controlled in differential pairs. By adjusting the values of R_1 through R_4 , the pressure at the intermediate nodes of

the bridge, P_1 and P_2 , are changed thereby modifying the flow, Q_1 and Q_2 , to the bellows. The differential pressure created at the intermediate nodes of the bridge is applied to the actuator plate, M_a , by the area enclosed by the bellows thus exerting force on the load mass, M_m .

Quiet hydraulics differs principally from conventional hydraulics in that the system is designed to maintain laminar flow, and there no frictional interfaces. In this way, a quiet hydraulic actuator can reach very low noise levels.

A schematic diagram for the quiet hydraulic actuator with a suspended load is shown in Figure 4. To avoid frictional interfaces, the cylinder and piston typical of conventional hydraulics is replaced with a pair of flexible bellows mounted to the actuator plate, M_a .

1.2 ACTUATOR DESIGN

Quiet hydraulic design seeks to avoid frictional and rolling interfaces. At the core of this philosophy are the stacked bellows that comprises the quiet hydraulic piston (Figure 4). Motion is constrained to the axial direction by two parallel motion flexures. A tripod flexure enables this piston design to operate in multi-degree-of-freedom systems (Figure 5).

Nominally, the parallel motion flexures guide the actuator plate in the direction of actuation. However, when the actuator is used in a multi-DOF system, the parallel motion flexures are used in combination with the tripod flexure to accommodate transverse motions. To this end, the tripod flexure is designed to be soft in rotations while stiff along the axis of actuation. When the tripod attach plate is translated off-axis, the actuator plate must tilt because of lateral constraint provided by the parallel motion flexures (Figure 5). Since there is a considerable axial distance between the tripod base and the actuator plate, the tripod attach plate may, nonetheless, translate laterally while remaining axially stiff.

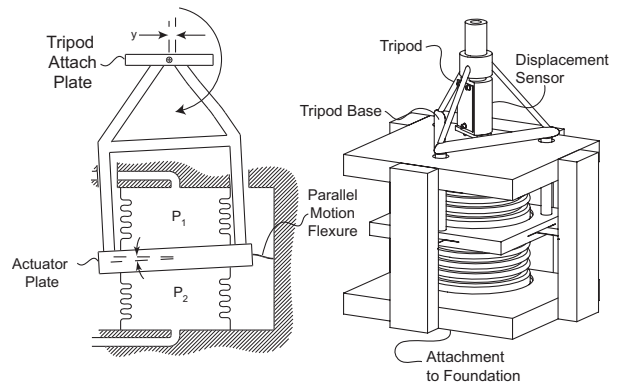


Figure 5: (1) (Left) Transverse motions, y , are accommodated by a tilting of the actuator plate and a rotation of the actuator attach plate. (2) (Right) The first prototype actuator.

2 HYDRAULIC RESONANCE

Based on the schematic representation of Figure 4, a one-dimensional mathematical model can be derived for the actuator’s frequency response [4]. Figure 6 compares the results of this model to data gathered from a prototype actuator on a single-axis platform. The prominent spike in the measured data is a mechanical resonance based on the compliance of the actuator and the mass of the payload. The model can reproduce the shape of the resonance by setting the bulk modulus of the fluid to be almost three orders of magnitude lower than that expected for the working fluid (even accounting for air entrapment). On further investigation of this discrepancy it was determined that the cause of the reduced resonant frequency is the *breathing stiffness* of the bellows. Breathing stiffness refers to the ability of a bellows to maintain a constant volume while the internal pressure is varied and the ends of the bellows are held fixed.

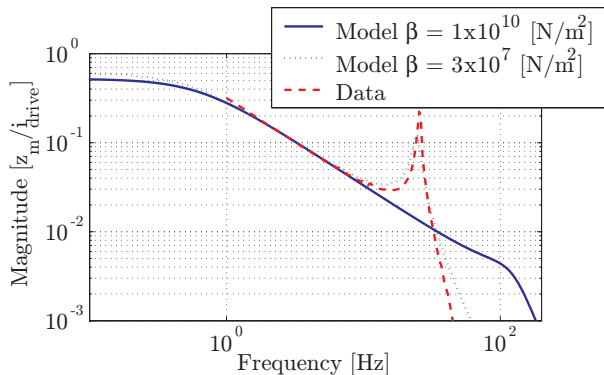


Figure 6: Driven transfer function of valve drive, i_{drive} , to mass position, z_m , measured by the displacement sensor. The model is shown for two values of bulk modulus, β , and compared to data.

The resonance shown in Figure 6 does not render the system uncontrollable. Indeed, performance exceeding the LIGO specification has been demonstrated (in one axis) with this peak inverted in the control law, but for long-term operation, such as in the final implementation at the LIGO site, stability and robustness are essential. Therefore, two approaches were adopted to passively mitigate this problem: redesign of the bellows and the addition of a bypass network.

2.1 BELLOWS DESIGN

A successful bellows design must maximize the breathing stiffness while maintaining axial compliance. The bellows of the prototype actuator performed poorly due to flat sections in the convolutions (Figure 7). Omitting the flats does improve the breathing stiffness, but at the cost of increased axial stiffness. The axial stiffness can be decreased by decreasing the wall thickness or increasing the length, but both of these choices impact the breathing stiffness.

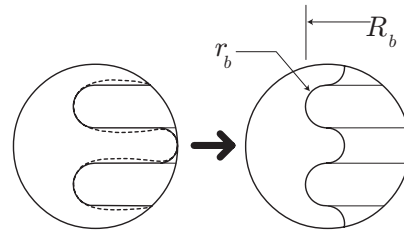


Figure 7: Close up details of the original bellows (left) and the new bellows (right). The dashed segments on the original design represent the distorted shape predicted by FE analysis of a 100 psi internal load.

Three parameters define the bellows geometry: the outside radius of the bellows, R_b ; the material thickness, t_b ; and the convolution radius, r_b (Figure 7). The relationship between these parameters is defined by the solutions of Roark (Table 30, Case 6b and 7b [5]) and Clark [6] (with some modification). The figure of merit for choosing a bellows design is the ratio of breathing stiffness to axial stiffness. This *stiffness ratio* is approximately 190 for the bellows on the prototype actuator.

For the purposes of control, it is desirable to move the hydraulic resonance past 50 Hz. This is twice the hydraulic resonant frequency of the prototype actuator which implies a 4x improvement in breathing stiffness, and given a constant axial stiffness, a stiffness ratio of roughly 800.

There are several limitations which bound the searchable space of the bellows geometry. The axial stiffness cannot increase and limit the available force from the actuator. The diameter and length of the bellows cannot exceed 12.5 cm (5 inches) so that overall size of the actuator does not become unwieldy. Lastly, for durability and fabrication, the material thickness cannot be thinner than 0.15 mm (0.006 in).

The approach taken here is, for each set of bellows dimensions, to calculate the number of convolutions needed to meet the axial compliance requirement. For that number of convolutions, the breathing stiffness is calculated, and the ratio of breathing to axial stiffness determined.

Figure 8 shows that decreasing the bellows’ convolution radius, r_b , and increasing the outside radius, R_b , increases the stiffness ratio. Decreasing the material thickness, t_b , also improves this ratio, but the prototype actuator bellows are already at the limit of 0.15 mm.

When the convolution radius, r_b , is very small, high numbers of convolutions will be required for the bellows to meet the axial compliance requirement. These high numbers of convolutions mean that the bellows will be longer than 12.5 cm, and hence, unsuitable for the actuator. The traces in Figure 8 are truncated before reaching these regions.

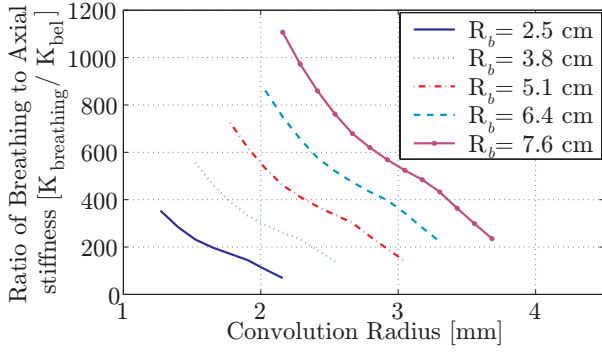


Figure 8: The effect of varying convolution radius and outside radius on the breathing to axial stiffness ratio for a bellows thickness of 0.15 mm (0.006 in.). The traces on the plot are not shown in the regions where the number of convolutions required to meet the axial stiffness limit cause the bellows to be too long.

Based on the results of Figure 8, the final dimensions chosen were outside diameter of 12.5 cm (5.0 in.), length of 12.5 cm (5.0 in.) and convolution radius of 2.1 mm (0.850 in.) with 12 convolutions. With these dimensions the breathing stiffness is predicted to improve from $1.70 \cdot 10^7$ N/m to $8.50 \cdot 10^7$ N/m for a new stiffness ratio of over 800.

Unfortunately, this improvement has been difficult to experimentally validate because the foundation supporting the actuator has a stiffness that is comparable to, or less than, the original breathing stiffness. Hence, the improvement from the updated bellows is as significant as desired (Figure 12).

2.2 THE BYPASS NETWORK

The search for a stiffer bellows revealed that it is difficult to achieve a 50 Hz natural frequency in the system because of the compliant foundation. An alternative approach is to passively damp the resonance by adding a bypass network.

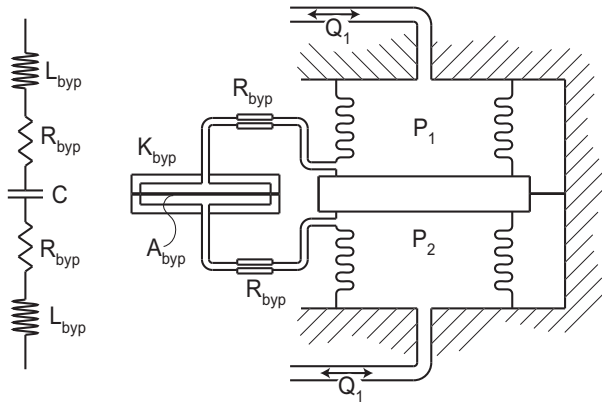


Figure 9: An electrical and schematic representation of the bypass network. The values of R_{byp} and C_{byp} are tuned to dissipate energy at the frequency of bellows'

breathing resonance. Parasitic inductance, L_{byp} limits the effective conductivity of the bypass resistors, hence limiting the upper corner frequency.

A bypass network is a path between the two bellows (Figure 9) with impedance to flow that varies with frequency. While there is no fluid exchange between the two bellows, at high frequencies the diaphragm becomes compliant and modulates a volume exchange between the two main chambers. This exchange draws fluid through the resistance, R_{byp} , and in so doing, dissipates energy in the form of heat.

The choice of frequency for the pole associated with the bypass network, $f_{byp} = \frac{1}{2\pi R_{byp} C_{byp}}$, is a compromise between control authority and suppression of the undesired resonance. Clearly, if the pole is set too low (the diaphragm compliance large), the actuator will cease to deliver the required force, and if the pole is too high, the suppression of the resonance will be minimal. For this actuator, the bypass pole frequency is set at 8 Hz.

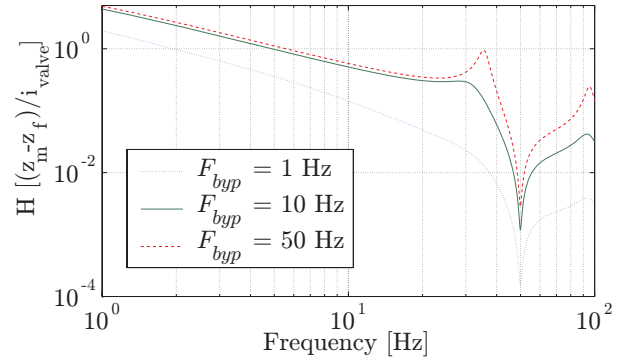


Figure 10: The transfer function from valve drive to platform displacement with various bypass pole frequencies.

Fluid inertia in passages of the bypass network introduces parasitic inductance and can prevent fluid from interacting with the diaphragm. This can render the bypass network useless. This effect is minimized by eliminating the passages and mounting the resistive elements directly to the diaphragm, but without careful design of these elements, the inductance of the resistive channels will dominate the network. Hence, the resistive channels must be designed such that the resistance of the channel dominates the inductance at the resonant frequency.

The design of a low inductance resistor is developed by setting the ratio of the inductive impedance to the resistive impedance equal to a small value, in this case $Ls/R = 0.01$ where s is set to be the frequency of the bellows' resonance. For cylindrical geometry, this expands to:

$$\frac{L_{round}s}{R_{round}} = \frac{4\rho \cdot length}{\pi \cdot diameter^2 s} = \frac{\rho \cdot diameter^2}{32\mu} s \quad (1)$$

where μ is the viscosity of the fluid. Solving for the diameter in equation 1 yields 1.64×10^{-4} m. For a desired

bypass resistance of $2 \times 10^9 \text{ Pa}\cdot\text{s}/\text{m}^3$, the associated length is $3.42 \times 10^{-7} \text{ m}$. This diameter is very small which will make the resistor sensitive to clogging, and since the diameter is larger than the length, it is unlikely that flow through the resistor will be fully developed.

Alternatively, the same ratio for a parallel plate resistor is:

$$\frac{L_{\text{parallel}}}{R_{\text{parallel}}} = \frac{\frac{\rho \cdot \text{length}}{\text{width} \cdot \text{height}}}{\frac{12\mu \cdot \text{length}}{\text{width} \cdot \text{height}^3}} = \frac{\rho \cdot \text{height}^2}{12\mu} \quad (2)$$

The parallel plate geometry offers an additional degree of freedom: the width. The height must still be small ($2.5 \times 10^{-4} \text{ m}$) to minimize the inductance, but the width may be adjusted to ensure that the length is ten times the height [7] to guarantee fully developed flow. Hence, the length is set to $2.5 \times 10^{-3} \text{ m}$ and width becomes 0.1 m.

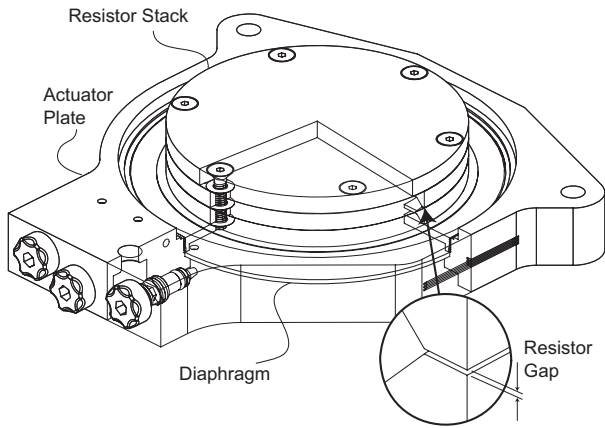


Figure 11: The resistor stack integrated to the actuator plate.

A width of 0.1 m is problematic because it is large by comparison to the size of the actuator. This is overcome by distributing the resistance around the periphery of a stack of rings (Figure 11). In this way, the resistor stack is well collocated with the diaphragm and fits inside the bellows.

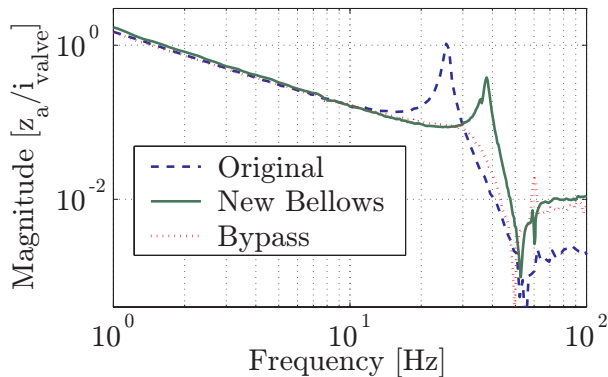


Figure 12: Suppression of hydraulic resonance with bypass network.

3 FINAL ACTUATOR DESIGN

The final actuator design incorporates the improved bellows design and the bypass network. This actuator also features an internal bleed network operated by six pin valves, and an updated tripod that is axially stiffer while maintaining the rotational softness by the addition of the tapered ends (Figure 13).

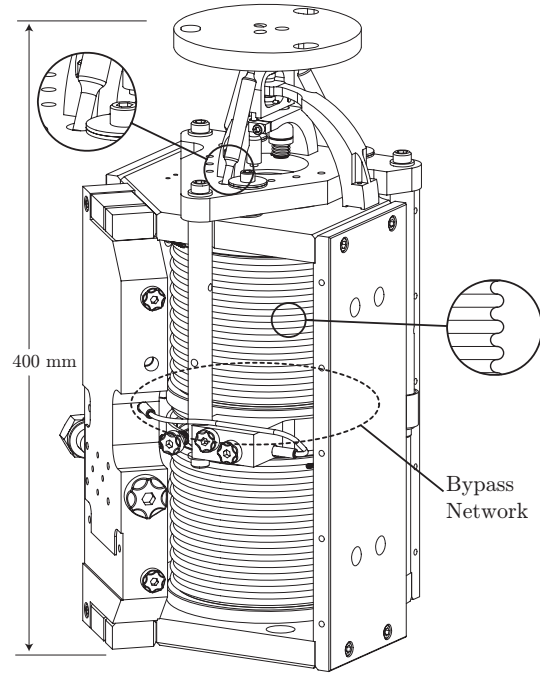


Figure 13: The final hydraulic actuator design. Note the tapered tripod flexures, integrated bypass network, and improved bellows convolution geometry.

4 IMPLEMENTATION IN LIGO

The purpose of the Hydraulic External Pre-Isolator (HEPI) system in LIGO is to provide 6 DOF alignment and 3 DOF isolation at low-frequency. To accomplish these requirements, each pier is outfitted with one vertical and one tangentially oriented (with respect to the circular chamber) horizontal actuator for a total of eight actuators. Only 6 actuators are necessary for 6 DOF control, but a 6 actuator system is not compatible with the 4-fold symmetry of the vacuum chamber (Figure 14). As a result, the system has two overconstrained modes, Overconstrained Vertical (OCV) and Horizontal (OCH).

Both alignment and isolation are required, and this can be best achieved by combining sensors designed for the different objectives. The alignment specification requires displacement feedback at low frequencies, while isolation requires inertial information used in either feed-forward or feedback. In order to achieve both of these somewhat conflicting goals, two less conventional controls techniques are applied: sensor blending and sensor correction.

have produced impressive results. Figure 16 shows the performance in the X direction (the interferometer axis) at LLO. Note that the microseismic peak at ~ 0.15 Hz. is reduced by a factor of 10 and this reduction continues up to 2 Hz.

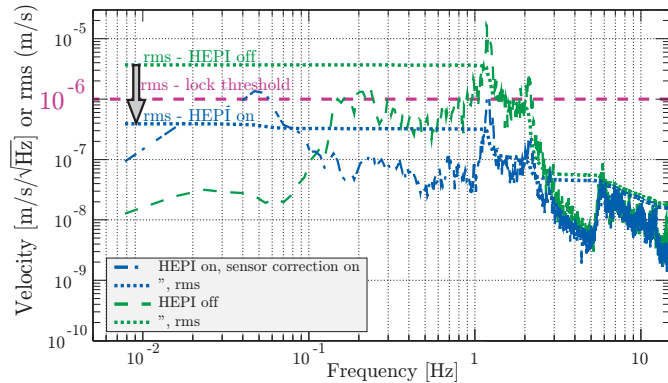


Figure 16: The impact of the HEPI system when applied to a 4 km Fabry-Perot cavity at LLO. The plot shows the differential velocity between the two mirrors, as corrected by the interferometer control. The solid curves show the amplitude spectral density with HEPI off (green) and on (blue). The dotted lines show the rms velocity integrated from high frequency to the frequency of interest. On a noisy day, the integrated velocity is about $3 \cdot 10^{-6}$ m/s rms with HEPI off, and $4 \cdot 10^{-7}$ m/s rms with HEPI on. The dashed line at $1 \mu\text{m/s}$ shows the typical threshold for locking. HEPI now allows LIGO to lock the interferometer, even on noisy days.[10]

6 Conclusions

The recent introduction of HEPI at LLO has already been recognized as a considerable improvement to the functionality of the observatory. Prior to the commissioning of HEPI, it was impossible for the interferometer to maintain lock during the daytime due to nearby logging activities. This meant that the observatory was only capable of producing useful data during the nighttime (in the absence of trains). After the installation of HEPI, it has been possible to maintain lock during the day even through the occasional passing freight train. Due to HEPI and other improvements, LLO has improved from operating 21.8 percent of the time (during science run 3) to over 74.5 percent (in science run 4) [11].

7 Acknowledgments

This material is based on work supported by the National Science Foundation under grants 9801158, 9900793, 0071316, 0107417, 0140297, and 0304924.

References

- [1] Abramovici et. al., “LIGO - The Laser Interferometer Gravitational-wave Observatory,” *Science*, 256, (1992), pp. 325-333.
- [2] E J Daw, J A Giaime, D Lormand, M Lubinski and J Zweizig, (7 May 2004) “Long-term study of the seismic environment at LIGO” *Quantum Grav.* 21 No 9, 2255-2273
- [3] D. Shoemaker, D. Coyne, “LIGO II Seismic Isolation Design Requirements Document,” LIGO internal document LIGO-E990303-02-D, Nov 4, 1999, <http://www.ligo.caltech.edu/docs/E/E990303-02.pdf>.
- [4] Hardham, Corwin (2006) “Quiet Hydraulics for LIGO”, Stanford PhD Thesis, Stanford University.
- [5] Roark and Young (1994). “Roark’s Formulas for Stress and Strain”, McGraw-Hill, Inc
- [6] Clark, R. A. (1950). “On the Theory of Thin Elastic Toroidal Shells”, *Journal of Mathematics and Physics*, vol. 29, no.3
- [7] White, Franklin (1994). “Fluid Mechanics”, Heightstown, New Jersey.
- [8] W Hua et al., (2004) “Low Frequency Active Vibration Isolation for Advanced LIGO”, in *Gravitational Wave and Particle Astrophysics Detectors*, Proceedings of SPIE, vol. 5500, p. 194.
- [9] W. Hua et al., (2004) “Polyphase FIR Complementary Filters for Control Systems”, *Spring Topical Meeting on Control of Precision Systems*, Proceedings ASPE, 32, 109.
- [10] J. Giaime (2004) “The X-arm interferometer test of HEPI at LIGO Livingston” LIGO internal document G040358-00-D.
- [11] S. Whitcomb, (2005) “State of the LIGO Lab”, LIGO internal document LIGO-G050395-00-M.